J|A|C|S
JOURNAL OF THE AMERICAN CHEMICAL SOCIETY

Article
pubs.acs.org/JACS

Semiquinone-Bridged Bisdithiazolyl Radicals as Neutral Radical Conductors

Xin Yu,[†] Aaron Mailman,[†] Kristina Lekin,[†] Abdeljalil Assoud,[†] Craig M. Robertson,[‡] Bruce C. Noll,[§] Charles F. Campana,[§] Judith A. K. Howard,[‡] Paul A. Dube,[‖] and Richard T. Oakley*,[†]

[†]Department of Chemistry, University of Waterloo, Waterloo, Ontario, Canada N2L 3G1
[‡]Department of Chemistry, University of Durham, Durham DH1 3LE, U.K.
[§]Bruker AXS, Inc., Madison, Wisconsin 53711, United States
[‖]Brockhouse Institute for Materials Research, McMaster University, Hamilton, Ontario, Canada L8S 4M1

Ⓢ *Supporting Information*

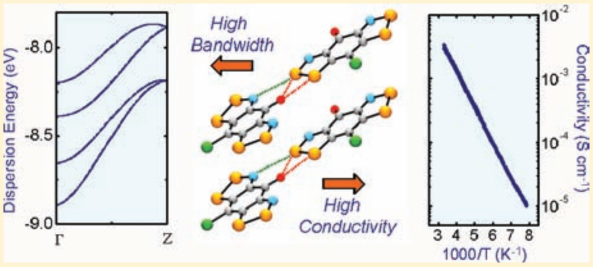

ABSTRACT: Semiquinone-bridged bisdithiazolyls **3** represent a new class of resonance-stabilized neutral radical for use in the design of single-component conductive materials. As such, they display electrochemical cell potentials lower than those of related pyridine-bridged bisdithiazolyls, a finding which heralds a reduced on-site Coulomb repulsion U. Crystallographic characterization of the chloro-substituted derivative **3a** and its acetonitrile solvate **3a**·MeCN, both of which crystallize in the polar orthorhombic space group $Pna2_1$, revealed the importance of intermolecular oxygen-to-sulfur (CO···SN) interactions in generating rigid, tightly packed radical π-stacks, including the structural motif found for **3a**·MeCN in which radicals in neighboring π-stacks are locked into slipped-ribbon-like arrays. This architecture gives rise to strong intra- and interstack overlap and hence a large electronic bandwidth W. Variable-temperature conductivity measurements on **3a** and **3a**·MeCN indicated high values of σ(300 K) (>10^{-3} S cm^{-1}) with correspondingly low thermal activation energies E_{act}, reaching 0.11 eV in the case of **3a**·MeCN. Overall, the strong performance of these materials as $f = {}^{1}/_{2}$ conductors is attributed to a combination of low U and large W. Variable-temperature magnetic susceptibility measurements were performed on both **3a** and **3a**·MeCN. The unsolvated material **3a** orders as a spin-canted antiferromagnet at 8 K, with a canting angle ϕ = 0.14° and a coercive field H_c = 80 Oe at 2 K.

■ INTRODUCTION

The conventional design strategy for inducing electrical conductivity in organic materials is based upon the use of charge transfer (CT) to generate charge carriers in otherwise closed-shell molecules.[1] As a result, conductive systems generally require two components, a donor and an acceptor, although it is possible to incorporate both partners into a single molecule.[2] The accumulated arsenal of semiconductors, metals and superconductors based on donors such as tetrathiafulvalene (TTF) and acceptors such as tetracyanoquinodimethane (TCNQ) and C_{60} attest to the success of the CT paradigm.[3,4] In addition, if one of the CT partners contains a transition metal[5] or possesses an attached "outrigger" radical,[6] materials can be made that display both conductive and magnetic signatures, a combination of potential value in the emerging field of molecular spintronics.[7]

Within the latter context, that is, the growing interest in spin-correlated conductivity, the pursuit of single-component molecular materials that possess both carriers of charge and spin holds much appeal.[8] In principle, molecular radicals represent ideal building blocks for such systems, and indeed, the possibility that the unpaired electron supplied by a neutral radical might serve as a charge carrier was proposed by Haddon more than 35 years ago.[9] In practice, however, the realization of conductivity in radical-based materials is not easy. For example, in light heteroatom (N, O) radicals such as aminyls, nitroxyls, and verdazyls, the spin density is too localized, and intermolecular hopping of the unpaired electrons is suppressed by a large on-site charge repulsion, causing such materials to be insulators.[10] Overcoming the charge repulsion problem, which can be understood within the language of Mott−Hubbard theory,[11,12] requires that nearest-neighbor interactions (expressed in terms of the intermolecular resonance integral β) be maximized and that the barrier to charge transport, the Mott−Hubbard on-site Coulomb repulsion parameter U, be minimized. When the electronic bandwidth W (= 4β)[13] is sufficient to offset charge repulsion, that is, when $W > U$, a metallic state should prevail. Toward this end, a wide range of delocalized polycyclic organic radicals, notably phenalenyls, spirophenalenyls,[14,15] and betainic CT radicals[3e,16] have been explored, but while high conductivity has been observed for some spirophenylenyls, a metallic ground state has yet to be achieved.

Received: October 19, 2011
Published: January 24, 2012

dx.doi.org/10.1021/ja209841z | *J. Am. Chem.Soc.* 2012, 134, 2264−2275

While light-heteratom radicals are poor conductors, the localization of spin density that suppresses charge transport serves to enhance magnetic properties by focusing the weak through-space intermolecular magnetic exchange interactions.[17] Indeed, the first nonmetal-based molecular ferromagnets were constructed from such building blocks.[18] However, the Curie temperatures of these systems are low ($T_C < 2$ K), and in the absence of spin−orbit coupling, magnetic anisotropy and the concomitant coercive fields H_c are essentially nonexistent. In an attempt to balance the potentially conflicting electronic requirements for charge transport and magnetic performance, that is, spin delocalization versus spin localization, strong versus weak (orthogonal) orbital overlap, we have pursued the development of heavy-heteroatom radicals, notably thiazyls and selenazyls, in the belief that the presence of nitrogen atoms in spin-bearing sites will suppress dimerization while orbital interactions between neighboring sulfur and selenium atoms, respectively, will generate pathways for charge migration and/or magnetic coupling. However, initial attempts to generate superimposed radical π-stacks from simple monocyclic thiazyl radicals afforded diamagnetic, Peierls-distorted[19] structures that were insulating or weakly semiconducting.[20]

A more serious problem with early, relatively localized thiazyl radicals was their high on-site Coulomb repulsion energy U.[21] Thus, even when dimerization could be avoided, intermolecular overlap between neighboring singly occupied molecular orbitals (SOMOs) and the resulting solid-state bandwidth W were insufficient to overcome charge repulsion, as a result of which the materials were trapped in Mott-insulating states. Improvements in conductivity could be induced by p-type doping,[22] which lowered U by changing the degree of band filling, but within the confines of the half-filled band ($f = {}^1/_2$) paradigm, the primary design challenge continues to be the development of new radical systems with more delocalized spin distributions and inherently low U values.

Chart 1

N-Alkylated pyridine-bridged bisdithiazolyl radicals **1** (Chart 1) were developed in response to this need for greater spin delocalization. As a result of the resonance stabilization effect,[15f] their gas-phase disproportionation energies ΔH_{disp} and electrochemical cell potentials E_{cell},[23] which provide indirect measures of U, are lower than those of simple monocyclic derivatives.[24] In addition, variations in the exocyclic groups R_1 and R_2 allow for fine-tuning of solid-state structures and hence intermolecular magnetic and electronic interactions.[25] However, most derivatives of this type crystallize as slipped π-stack arrays of radicals locked into herringbone packing patterns, a motif that compromises bandwidth and hence charge transport. As a result, their room-temperature conductivities σ_{RT} are on the order of 10^{-6}–10^{-5} S cm^{-1}. However, replacement of sulfur by its heavier congener selenium[26] increases the bandwidth by virtue of the greater spatial extension of the 4p orbitals on selenium relative to the 3p orbitals on sulfur, resulting in improved conductivity. Moreover, the introduction of spin−orbit coupling effects[27] occasioned by the presence of the heavy heteroatom selenium gives rise to some remarkable magnetic effects, including Dzyaloshinsky−Moriya spin canting[28] and hard ferromagnetism,[29] with T_C values as high as 17.5 K at ambient pressure and rising to 24 K at 2 GPa.[30]

In an attempt to break away from the herringbone mold found for **1**, we explored the structures of N-alkylated pyrazine-bridged radicals **2**. While removal of the steric protection afforded by the basal ligand makes these radicals more susceptible to dimerization, as in **2b** (R = Et),[31] we were eventually able to prepare radical **2a** (R = Me), which displays a superimposed but alternating ABABAB π-stack structure[32] whose electronic bandwidth and hence conductivity are both dramatically improved relative to those seen in the herringbone structures found for **1**. However, at low temperatures (<120 K), the evenly spaced π-stacks of **2a** collapse into dimers, thereby producing a diamagnetic ground state. As a continuation of these efforts to move away from the herringbone packing of the π-stacks found in **1** while at the same time avoiding the spin-quenching dimerization found for **2**, we have explored the effect on structure and function of the isoelectronic replacement of the NR_1 moiety in **1** with a carbonyl group to produce the resonance-stabilized semiquinone-bridged bisdithiazolyl system **3**. While the molecular electronic structure of these new radicals is similar to that of both **1** and **2**, the polarity of the carbonyl CO bond in **3** leads to the development of strong intermolecular S···O′ interactions in the solid state, and these supramolecular synthons[33] give rise to more rigid, more tightly bound frameworks that display improved charge transport properties. Following the synthetic procedure developed for the recently reported phenyl-substituted derivative **3b** (R = Ph),[34] we have now prepared the corresponding chloro-substituted compound **3a** (R = Cl). In the present paper, we describe the spectroscopic, electrochemical, and structural characterization of **3a** and its acetonitrile solvate **3a**·MeCN. Variable-temperature magnetic susceptibility and conductivity measurements are also reported, and the results are interpreted in the light of Extended Hückel Theory (EHT) electronic band structure calculations.

■ RESULTS

Building Block Synthesis. The general preparative route to semiquinone-bridged bisdithiazolyls **3** starts from the appropriate 4-substituted phenol **4** (Scheme 1), which can be readily oxidized with nitric acid to the corresponding 2,6-dinitrophenol **5**. Reduction of **5** with Sn/HCl then yields the

Scheme 1

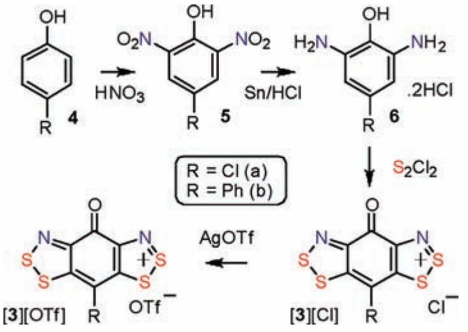

bishydrochloride of 2,6-diaminophenol **6**, which undergoes a double Herz cyclization with sulfur monochloride in MeCN at reflux to afford the chloride salt [**3**][Cl] as an insoluble blue-black solid.[35] This crude material may be converted into more soluble triflate ($CF_3SO_3^-$ or OTf^-) and/or hexafluoroantimonate (SbF_6^-) salts by metathesis with AgOTf or $AgSbF_6$. Solutions of salts of $\mathbf{3}^+$ in MeCN are deep-blue in color, although the associated absorption maxima (see the Experimental Section) are somewhat blue-shifted relative to those observed for salts of $\mathbf{1}^+$.

Electrochemistry. To determine suitable chemical reducing agents for the generation of **3**, we explored its electrochemical behavior by cyclic voltammetry (CV), starting from solutions of [**3**][OTf] in MeCN with 0.1 M n-Bu_4NPF_6 as a supporting electrolyte and Pt wire electrodes. As may be seen in Table 1, there are some differences in the half-wave potentials for the reversible 0/+1 couples of **3a** and **3b** that can be related to changes in the electron-withdrawing power of the axial ligand R; similar trends have been observed for derivatives of **1**.[36] More importantly, the results establish that both semiquinone-bridged salts [**3**][OTf] are more easily reduced (by about 200 mV) than the corresponding pyridine-bridged materials [**1**][OTf]. For the second reduction process, which corresponds to the −1/0 couple, the difference between the two systems is more profound. Not only is there a large anodic shift in the half-wave potential (nearly 400 mV) upon moving from **1** to **3**, but in the latter case, the reduction wave is strongly irreversible (Figure 1). This irreversibility, which is independent of scan rate and sample concentration, may stem from comproportionation of the electrochemically produced anion with (excess) bulk cation, a phenomenon that has been observed in the electrochemistry of simple monocyclic dithiazolylium cations[37] and related materials.[21b,38] In view of the irreversibility of the −1/0 couple, it is more difficult to establish the corresponding cell potentials E_{cell} for **3a** and **3b**. We can nonetheless make an upper-limit estimate of the magnitude of E_{cell} by taking the difference in the E_{pc} values for the −1/0 and 0/+1 couples, and by so doing E_{cell} was found to be near 0.60 V for both radicals, which is substantially lower than that observed (near 0.80 V) for **1** (Table 1).

Table 1. Electrochemical Potentials[a] for 1 and 3

	$E_{1/2}(-1/0)$[b]	$E_{1/2}(0/+1)$[b]	E_{cell}[c]
1 (R_2 = Cl)[d]	−0.835	0.005	0.84
1 (R_2 = Ph)[e]	−0.956	−0.104	0.85
3a (R = Cl)	−0.481[f]	0.195 (0.158)[g]	0.64[h]
3b (R = Ph)[i]	−0.529[f]	0.108 (0.071)[g]	0.60[h]

[a] In volts, measured in MeCN. [b] Referenced to SCE. [c] $E_{cell} = E_{1/2}(0/+1) - E_{1/2}(-1/0)$. [d] R_1 = Me; see ref 25b. [e] R_1 = Me; see ref 36. [f] Irreversible reduction; only the cathodic peak potential E_{pc} is cited. [g] $E_{1/2}$; E_{pc} is given in parentheses. [h] E_{cell} estimated as $E_{pc}(0/+1) - E_{pc}(-1/0)$. [i] From ref 34.

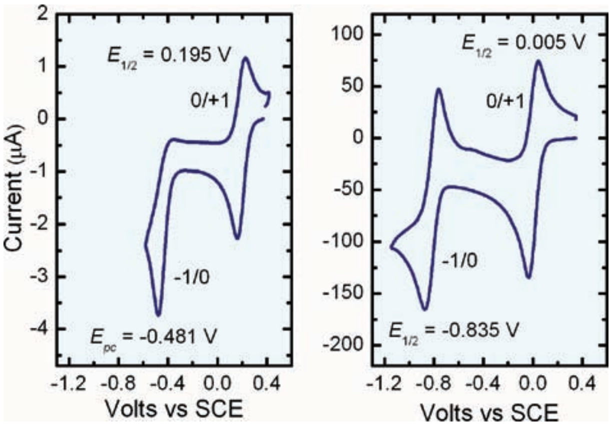

Figure 1. CV scans of (left) [**3a**][OTf] and (right) [**1a**][OTf] in MeCN with 0.1 M n-Bu_4NPF_6 supporting electrolyte. Data for [**1a**][OTf] were taken from ref 25b.

Isolation of Radicals. On the basis of the half-wave potentials observed for the 0/+1 couples for **3a** and **3b** and our experience with the chemical reduction of salts of $\mathbf{1}^+$ to the respective radicals **1**, we initially selected octamethylferrocene (OMFc) [$E_{1/2}$(ox) = −0.038 V vs SCE][29,39] as a suitable reagent to convert [**3a**][OTf] and [**3b**][OTf] to the corresponding radicals. This proved to be an ideal choice for **3b**, which was readily obtained as black needles by codiffusion of MeCN solutions of OMFc and [**3b**][OTf] in a glass H-cell. Crystallization of radical **3a** proved to be a more challenging exercise but eventually a more productive one. Initial attempts to reduce [**3a**][OTf] with OMFc using H-cell techniques and MeCN as the solvent afforded a microcrystalline precipitate displaying a weak IR band near 2200 cm^{-1}, the presence of which led us to suspect (correctly) the formation of an acetonitrile solvate. To produce larger crystals of this material, we explored the use of milder reducing agents, including dimethylferrocene (DiMFc), whose potential (0.263 V vs SCE)[29,40] is by itself insufficient to reduce [**3a**][OTf]. However, in practice, and aided by lattice energy (solvation) effects, DiMFc functioned perfectly, affording fine black needles of the acetonitrile solvate **3a**·MeCN when added slowly to solutions of [**3a**][OTf] in acetonitrile. The structure of this material is described below.

With the isolation of **3a**·MeCN successfully completed, the question then arose as to whether it might be possible to generate crystals of the unsolvated radical **3a**. To this end, we considered alternative solvents, eventually settling on propionitrile (EtCN). However, this choice required that we switch counteranions, as [**3a**][OTf] displayed insufficient solubility in EtCN. Success was finally achieved using [**3a**][SbF_6] as the precursor salt and OMFc as the reducing agent. This combination afforded **3a** as very small splintered needles that were shown by IR and elemental analysis to be free of solvent. Single-crystal and powder X-ray diffraction studies and transport property measurements were performed on this material.

EPR Spectra. The spin distribution in radicals of type **3** has been explored by EPR spectroscopy. In our earlier communication, we reported the X-band EPR spectrum of **3b**,[34] which consists of a broad five-line pattern arising from hyperfine coupling to two equivalent dithiazolyl nitrogens [$I(^{14}N) = 1$], the value of a_N (0.352 mT) being similar to, although slightly larger than, that observed for **1b** (0.320 mT).[36] Likewise, solutions of **3a**, obtained by dissolving crystals of either unsolvated **3a** or its MeCN adduct in toluene or dichloromethane, display a strong five-line EPR signal (Figure 2) reminiscent of that observed for the related pyridine-bridged radical **1a**.[25b] For both systems, the a_N values (Table 2) are approximately one-half of those found in monofunctional 1,2,3-dithiazolyls, as would be expected given the fact that the spin density is "shared" between two dithiazolyl rings.[41]

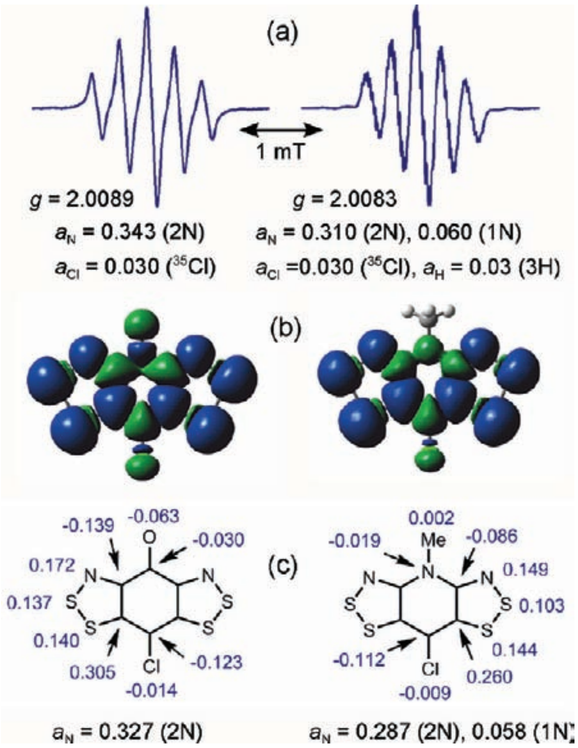

Figure 2. (a) X-band EPR spectra (spectral width = 3.0 mT) of (left) **3a** and (right) **1a** in toluene; hyperfine coupling constants *a* in mT are shown. (b) Kohn−Sham spin density isosurfaces and (c) atomic spin densities ρ and a_N values (in mT) derived from single-point UB3LYP/EPR-III/6-31G(d,p) calculations at the UB3LYP/6-311G(d,p)-optimized geometries.

Table 2. Computed[a] Ion Energetics

	3a	1a
IP	6.66	6.31
EA	2.04	1.78
$\langle S^2 \rangle$	0.8141	0.7797
ΔH_{disp}[b]	4.62	4.53
EN[c]	2.16	2.03

[a] Gas-phase ΔSCF values in eV from (U)B3LYP/6-311G(d,p) calculations. [b] ΔH_{disp}= IP − EA. [c] Mulliken electronegativity EN = (IP + EA)/2.

We also compared the spin distributions in the semiquinone- and pyridine-bridged radicals obtained using density functional theory (DFT) calculations at the UB3LYP/EPR-III/6-31G-(d,p) level. Illustrations of the Kohn−Sham spin density isosurfaces of **3a** and **1a** are shown in Figure 2, along with numerical details for each. The results support the qualitative similarity of the two radicals but also reveal some potentially important differences. For example, not only is the spin density on nitrogen (ρ_N = 0.172) in **3a** greater than that in **1a** (ρ_N = 0.149), in accord with the observed (and calculated) a_N values, but so too is ρ_S for the thiazyl sulfur (Figure 2). Both of these features are consistent with the possibility of stronger intermolecular magnetic and electronic interactions for the semiquinone-bridged radical. We also used DFT methods to compare the gas-phase ion energetics of the two systems. As shown in Table 2, the calculated ionization potential (IP), electron affinity (EA), and Mulliken electronegativity (EN) of **3a** are greater than those of **1a**; these results are consistent with the electrochemical potentials and indicative of the electron-withdrawing effect of the carbonyl group. Somewhat surprisingly, however, the gas-phase disproportionation energies (ΔH_{disp}) of **3a** (4.62 eV) and **1a** (4.53 eV) are almost identical. This finding, which is inconsistent with the experimental cell potentials E_{cell} (Table 1), may simply reflect the difficulty of the hybrid B3LYP functional in handling spin correlation in the semiquinone system, a problem suggested by the higher level of spin contamination ($\langle S^2 \rangle$) found in **3a**.

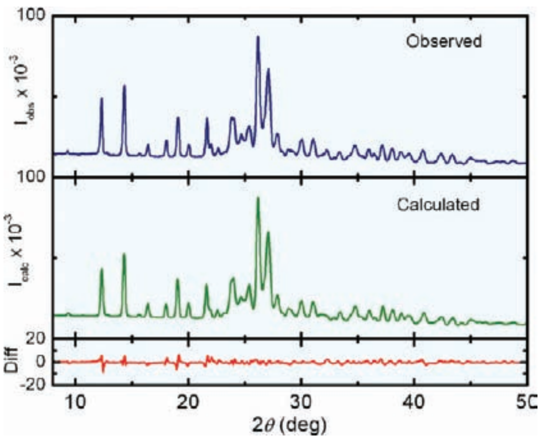

Figure 3. Observed and calculated powder X-ray diffraction patterns for unsolvated **3a** (λ = 1.5406 Å).

Table 3. Crystal Data

compound	[3a][SbF$_6$]·MeCN	3a·MeCN	3a
formula	$C_8H_3ClF_6N_3OS_4Sb$	$C_8H_3ClN_3OS_4$	$C_{18}Cl_3N_6O_3S_{12}$
M	556.57	320.82	839.43
a (Å)	14.3729(7)	9.4913(3)	48.779(3)
b (Å)	14.3342(7)	23.5986(8)	3.8228(2)
c (Å)	16.5005(8)	5.3124(2)	14.2036(9)
V (Å^3)	3399.5(3)	1189.88(7)	2648.6(3)
ρ_{calcd} (g cm^{-1})	2.179	1.791	2.105
space group	*Pbca*	*Pna*2$_1$	*Pna*2$_1$
Z	8	4	4
T (K)	296(2)	300(2)	100(2)
μ (mm^{-1})	2.335	9.300	12.373
λ (Å)	0.71073	1.54178	1.54178
data/restr./ parameters	4096/30/267	1770/1/155	2785/400/423
solution method	direct	direct	direct
R, R_w (on F^2)	0.0458, 0.0803	0.0216, 0.0561	0.0808, 0.2027

Crystallography. The crystal structures of the semiquinone-bridged radical **3a** and its acetonitrile solvate **3a**·MeCN were determined by single-crystal X-ray diffraction. Given the small size of the crystals of the unsolvated radical and the consequent paucity of reflections and relatively high *R* values, we cross-checked the single-crystal results by powder diffraction analysis (Figure 3).[42] This experiment also confirmed the phase uniformity of the bulk material. Table 3 lists crystal data, while Figure 4 illustrates ORTEP drawings of the asymmetric units of **3a** and **3a**·MeCN and provides the atom-numbering schemes; selected intramolecular metrics are provided in Table 4. To check the effect of redox changes on the internal structural parameters, we also structurally

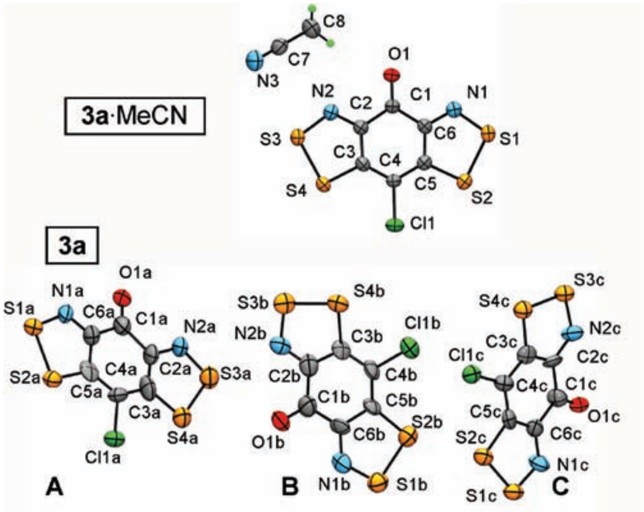

Figure 4. ORTEP drawings (50% probability ellipsoids) of the asymmetric units of unsolvated **3a** and **3a**·MeCN, showing the atom-numbering schemes. The three crystallographically distinct radicals in **3a** are labeled **A**, **B**, and **C**.

characterized the salt [**3a**][SbF_6]·MeCN. This revealed small contractions in the S−S, S−N, and S−C distances in the cation relative to those seen in the radical. Similar variations between the cation and radical oxidation states of **1** were observed and can be related to the removal of an electron from a predominantly antibonding SOMO.[25]

Table 4. Internal Metrics[a]

compound	[**3a**][SbF_6]·MeCN	**3a**·MeCN	**3a**[b]
S−S	2.062(2)	2.093(4)	2.10(4)
S−N	1.593(4)	1.625(2)	1.59(6)
N−C	1.316(4)	1.312(8)	1.32(4)
S−C	1.703(4)	1.732(12)	1.73(8)
C−O	1.217(4)	1.216(3)	1.21(3)

[a] Distances in Å; for averaged values, the numbers in parentheses are the greater of the difference and the standard deviation. [b] Averaged over three molecules.

Crystals of the acetonitrile solvate **3a**·MeCN possess an orthorhombic structure with $Z = 4$ and display a π-stacked architecture in which the molecules are linked laterally into coplanar arrays by intermolecular S···O′ and S···N′ contacts. As shown in Figure 5, the cell dimensions and symmetry of the $Pna2_1$ space group dictate a packing pattern in which the radicals in the coplanar arrays are aligned in regular (not alternating) slipped π-stacks running along the *z* direction. Nearest neighbors along *x* and *y* are related by *n*-glide planes, producing a cross-braced appearance when the π-stacks are viewed along the *y* direction. Each of the 2D arrays of π-stacks comprises ribbons of radicals inclined in the same direction (*not* in a herringbone pattern) at an angle $\theta = 49.6°$ with respect to the *c* axis. Within each ribbon, neighboring radicals are linked by short S···O′ and S···N′ contacts that defined numerically in the Supporting Information. The interlocking of the radicals by these supramolecular synthons[33] produces a zigzag or wavelike array within the folds of which the acetonitrile solvate molecules are perfectly sequestered; the radicals and solvent molecules are locked together by short polar MeCN···S′ interactions. There are no intermolecular contacts inside the van der Waals separation[43] between radicals in neighboring π-stacks along *y*, although there is one interaction (S1···S2′ = 3.750 Å) that may provide some interstack electronic communication.

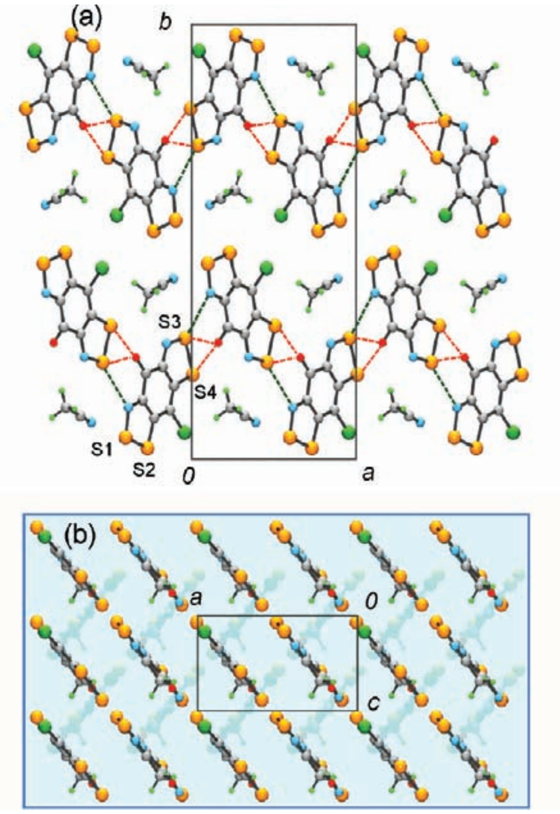

Figure 5. Unit cell of **3a**·MeCN viewed parallel to (a) the *c* axis and (b) the *b* axis. In (b), the layer with $y < 0.5$ is shaded. Intermolecular S···O′ (red) and S···N′ (green) contacts are shown with dashed lines.

Inspection of the ribbonlike layers within the π-stacks of **3a**·MeCN reveals some interesting features that may be compared to the herringbone structures observed for radicals of type **1**. For example, as illustrated in Figure 6, there is considerable π-type overlap between radicals in neighboring stacks of **3a**·MeCN. This feature is not possible in a herringbone packing pattern. The mean planes of radicals along the π-stacks of **3a** are separated by a distance $\delta = 3.497$ Å, which is similar to the interplanar separations seen in radical π-stacks of **1**, although there is no single interatomic separation that lies within the standard van der Waals separation.[43] The electronic consequences of this arrangement are developed below.

Like the acetonitrile adduct **3a**·MeCN, crystals of the unsolvated radical **3a**, as grown from propionitrile, belong to the polar orthorhombic space group $Pna2_1$. The crystal architecture of the two variants is, however, profoundly different. There are three independent molecules (**A**, **B**, and **C**) in the asymmetric unit of **3a** (Figure 4), and with $Z = 4$, this gives rise to a total of 12 molecules in the unit cell. Each of the three radicals **A**, **B**, and **C** forms the basis for an evenly spaced, slipped π-stack running parallel to the *b* axis. The unit cell drawing provided in Figure 7 illustrates the packing of the radicals in the *xz* plane. Also indicated in this drawing is the labyrinth of lateral intermolecular S···S′, S···O′, and S···N′ contacts that stitch the radicals together. All of these contacts, which are defined numerically in the Supporting Information,

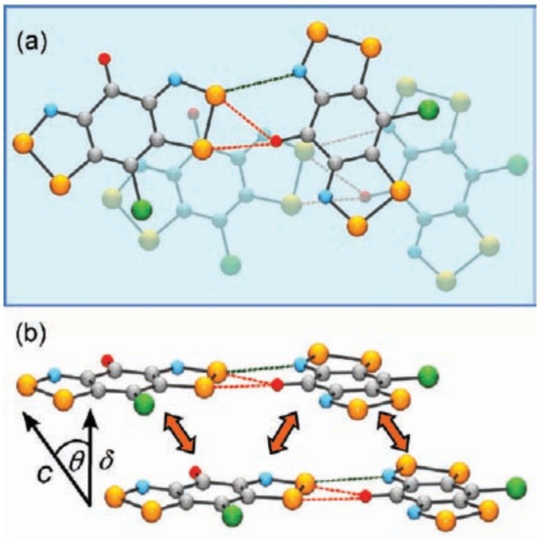

Figure 6. Two views of slipped π-stacks in **3a**·MeCN: (a) view perpendicular to the molecular planes; (b) side view illustrating interlayer interactions along and between the π-stacks. Intermolecular S···O′ (red) and S···N′ (green) contacts are shown with dashed lines.

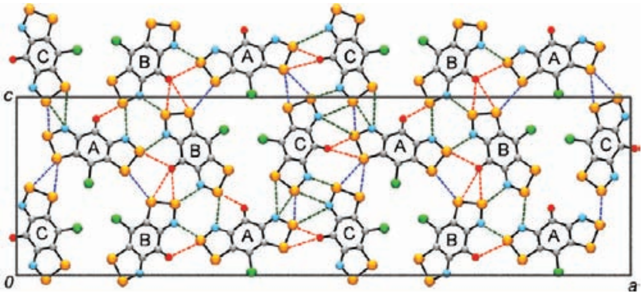

Figure 7. Packing of **A**, **B**, and **C** radicals in the *xz* plane of the unit cell of unsolvated **3a**, showing lateral intermolecular S···S′ (blue), S···O′(red), and S···N′ (green) contacts.

are within the respective van der Waals separations.[43] The overall structural motif can be described in terms of wavelike arrays of **C** radicals that weave along the *z* direction, neighboring molecules being related by 2_1 axes at $x = 0$ and $^1/_2$ and linked by four-center $(S\cdots N')_2$ secondary-bonding[44] bridges. The **B** radicals also form wavelike arrays along the *z* direction, but nearest neighbors are now related by the *n*-glides at $x = {}^1/_4$ and $^3/_4$ and are linked by S···O′ and S···N′ contacts. Finally, the **A** radicals serve as bridges between these two chains, interacting strongly with each.

Despite the rather oblique alignment of the three independent π-stacks, when they are viewed parallel to the *z* direction (Figure 8), close examination reveals that the individual columns share common features. First, in all three π-stacks, the interplanar separation δ is closer than that seen in **3a**·MeCN and nearer to the value observed in graphite.[45] Second, slippage of the radicals occurs almost exclusively by a longitudinal movement of neighboring radicals, as indicated by the value of d*y* in Table 5; the small value of d*x* coupled with the almost equal intermolecular S1···S2′ and S3···S4′ interactions indicates virtually no lateral slippage. Staggering of this type and to this degree has been seen before in π-stacked radicals of type **1**[25b] and in those systems was associated with relatively weak (orthogonal) intrastack overlap.

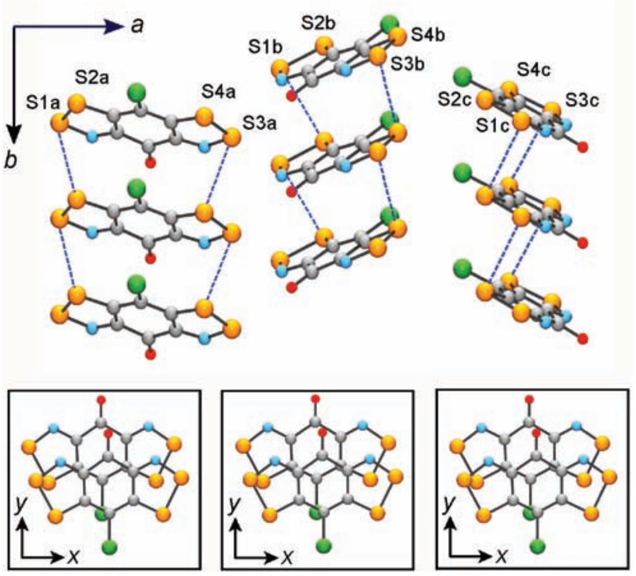

Figure 8. Slipped π-stacking of the three symmetry-independent radicals in unsolvated **3a**. Staggering of the radicals affords close intracolumnar S1···S2′ and S3···S4′ interactions. The views at the bottom illustrate the slippage of adjacent radicals along the local directions *x* and *y*.

Table 5. Structural Parameters[a] of the π-Stacks in 3a

compound	radical **A**	radical **B**	radical **C**
S1···S2′	3.633	3.453	3.545
S3···S4′	3.574	3.625	3.575
δ[b]	3.374	3.359	3.368
d*x*[c]	0.300	0.249	0.231
d*y*[d]	1.771	1.808	1.792

[a] All distances in Å. [b] Interplanar separation along π-stacks. [c] Lateral slippage in the *x* direction of neighbors along π-stacks (see Figure 8) . [d] Longitudinal slippage in the *y* direction of neighbors along π-stacks (see Figure 8) .

Band Structures. To explore and compare the electronic structures of the radicals of **3a** and **3a**·MeCN, we carried out a series of EHT band structure calculations on the crystal structure geometries. The results must be viewed with caution, as the tight-binding approximation fails to provide a proper description of the ground state of strongly correlated systems such as these. The method nonetheless provides qualitative insight into the direction and extent of intermolecular orbital interactions within and between the radical π-stacks. As in previous work, we focused on the dispersion of the crystal orbitals (COs) arising from the interactions of the SOMOs along the π-stacking direction.[46] Idealized views of this antibonding A_2 symmetry orbital are illustrated in Figure 9.

The results are summarized in Figure 10 in the form of dispersion curves for the SOMO-based COs, which collectively would constitute the $f = {}^1/_2$ band if the ground state were metallic. Inasmuch as the number of bands reflects the number

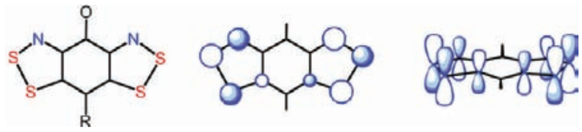

Figure 9. Idealized views of the A_2 π-SOMO of **3**.

of molecules in the unit cell, there are four bands for **3a**·MeCN but a total of 12 for unsolvated **3a**. In each case, the spread of the set of COs across the Brillouin zone gives a qualitative estimate, within the tight-binding approximation, of the solid-state bandwidth. On this basis, it is immediately apparent that the bandwidth $W = 1.02$ eV found for the acetonitrile adduct **3a**·MeCN is exceptionally large. Moreover, the strong dispersion observed along a^* ($\Gamma \rightarrow X$) and c^* ($\Gamma \rightarrow Z$) also indicates a well-developed two-dimensional (2D) electronic structure, in accord with the slipped-ribbon architecture illustrated in Figure 5b. In contrast, the unsolvated material **3a** shows only limited interactions along the π-stacks ($\Gamma \rightarrow Y$) and even weaker dispersion along the remaining two principal directions of reciprocal space. Overall, the bandwidth W is estimated to be 0.52 eV. The EHT electronic bandwidths for the radicals thus clearly indicate the ribbonlike π-stacked architecture of the solvated material as having the most well-developed electronic structure, the one most likely to confer high conductivity. In contrast, in the unsolvated structure, the interactions are weaker, in terms of both magnitude and directionality, and indeed are reminiscent of those seen in the herringbone structures of pyridine-bridged radicals **1**.

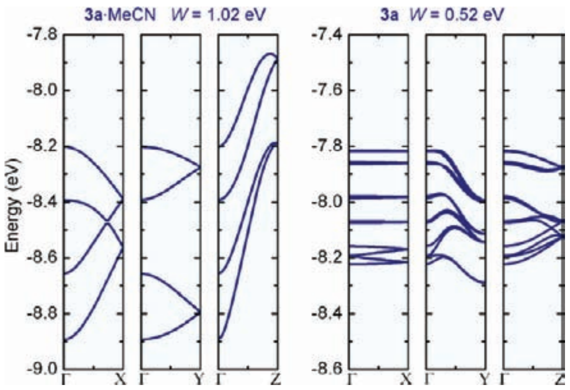

Figure 10. EHT dispersion curves for (left) **3a**·MeCN and unsolvated (right) **3a**.

Magnetic Properties. Previously reported variable-temperature direct current (DC) magnetic susceptibility (χ) measurements[34] on **3b** taken at low field ($H = 100$ Oe) over the range 2–300 K indicated strong local ferromagnetic (FM) coupling along the π-stacks. Analysis of the data over the range $T = 6$–30 K in terms of the Baker model[47] for a Heisenberg 1D FM-coupled chain (π-stack) of $S = {}^1/_2$ centers yielded exchange coupling constants $J = +29.5$ cm^{-1} for interactions along the π-stacks and $zJ' = -2.5$ cm^{-1} for the cumulative interstack (mean-field) interactions. Upon further cooling, the FM chains become aligned in an antiparallel fashion to form a spin-canted antiferromagnetic (AFM) state with a Néel temperature (T_N) of 4.5 K. With increasing field, the AFM chains undergo a spin-flop transition to a field-induced FM state.

Here we carried out similar magnetic measurements on **3a**·MeCN and unsolvated **3a** (Table 6). The data for **3a**·MeCN, illustrated in Figure 11 in the form of cooling curve plots of χ and χT versus T measured using an external field of $H = 1$ kOe, indicated strongly antiferromagnetically coupled paramagnetic behavior. Consistently, the results of a Curie–Weiss fit over the range 100–300 K afforded a large negative θ value (−61.7 K). There was no evidence, however, for a structural or magnetic phase transition upon cooling the sample to 2 K. The high-temperature cooling curve data (with $H = 1$ kOe) for the unsolvated material **3a** (Figure 12) also suggested an antiferromagnetically coupled Curie–Weiss paramagnet with $\theta = -27.0$ K, but upon cooling below 10 K, this material displayed a rapid increase in both χ and χT. The surge was more pronounced at lower field ($H = 100$ Oe), and a subsequent zero-field-cooled/field-cooled (ZFC/FC) experiment revealed a sharp bifurcation in $\chi(T)$ at 8 K for the ZFC and FC sweeps, indicative of a phase transition to a spin-canted antiferromagnetically ordered state with $T_N = 8$ K. Field-independent magnetization experiments confirmed the ordering temperature, and back-extrapolation of M to $T = 0$ K afforded a value of the spontaneous magnetization $M_{\mathrm{spont}} = 2.5$ mNβ, which was used to estimate the spin-canting angle $\phi = 0.14°$.[48] Measurements of M as a function of field were also performed, and these indicated a weak, quasi-linear M versus H dependence out to 5 T. Cycling of the field revealed a subtle but distinct hysteretic response in $M(H)$, giving rise to a coercive field $H_c = 80$ Oe at 2 K.

Table 6. Conductivity and Magnetic Parameters

	3a·MeCN	3a	3b[a]
σ(300 K) (S cm^{-1})	3.0×10^{-3}	4.0×10^{-3}	3.0×10^{-5}
E_{act} (eV)	0.11	0.16	0.20
C (emu K mol^{-1})	0.389	0.351[b]	0.349[b]
θ (K)	−61.7	−27.0[b]	32.8[b]
T_N (K)	–[c]	8.0	4.5

[a] See ref 34. [b] From a Curie–Weiss fit to the 100–300 K data. [c] Does not order magnetically above 2 K.

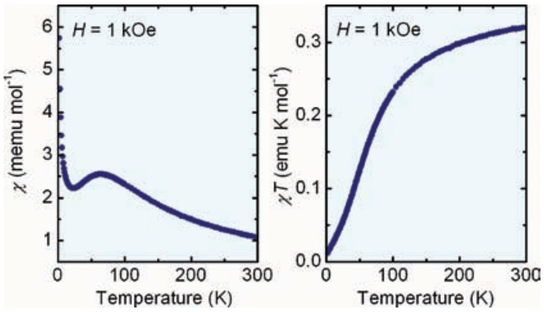

Figure 11. Field-cooled (left) χ versus T and (right) χT versus T plots for **3a**·MeCN at $H = 1$ kOe.

Conductivity Measurements. We reported previously the results of variable-temperature conductivity (σ) measurements on **3b**.[34] Similar measurements using the four-probe method on cold-pressed pellets were performed here on **3a**·MeCN and unsolvated **3a**. The results are persented in Figure 13 in the form of plots of log σ against $1/T$. Values of σ(300 K) and the Arrhenius activation energy E_{act} are summarized in Table 6 along with the results of measurements previously reported for **3b** and **1a**. Comparison of the performance of **3a**, **3a**·MeCN, and **3b** with that of related pyridine-bridged materials, of which **1a** is representative,[25b] indicates that the semiquinone-bridged materials are uniformly superior in terms of both enhanced conductivity and lowered activation energy. Indeed, the values of σ(300 K) for **3a** and **3a**·MeCN are among the highest ever observed for a neutral $f = {}^1/_2$ radical. Not only are they several orders of magnitude higher than those for radicals of type **1**, for which σ(300 K) is generally in the range 10^{-6}–10^{-5} S cm^{-1}, but they also rival that of the very best selenium-based variant of **1**, namely, 5×10^{-3} S cm^{-1} when R_1 = Me, R_2 = Cl.[49] Moreover,

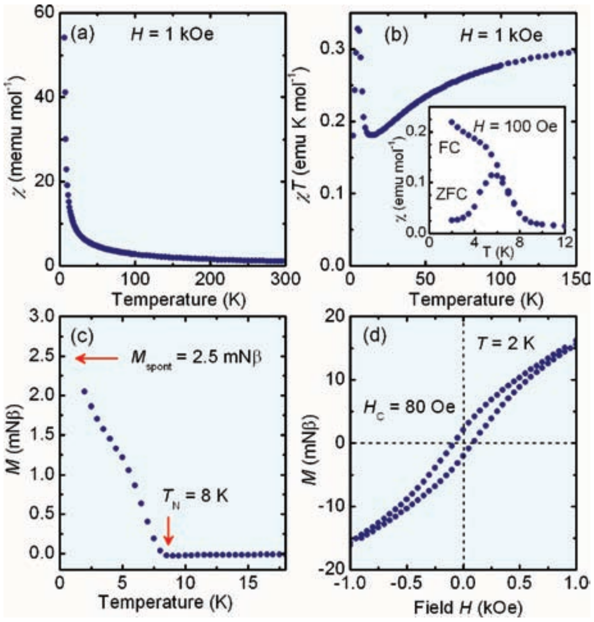

Figure 12. (a) Field-cooled χ versus T plot for unsolvated **3a** at $H = 1$ kOe. (b) Field-cooled χT versus T plot for unsolvated **3a** at $H = 1$ kOe. The inset shows a ZFC/FC plot of χ versus T at $H = 100$ Oe. (c) Decay of the spontaneous magnetization M with increasing temperature for unsolvated **3a**. (d) Hysteresis in cycling of M versus H measurements at $T = 2$ K.

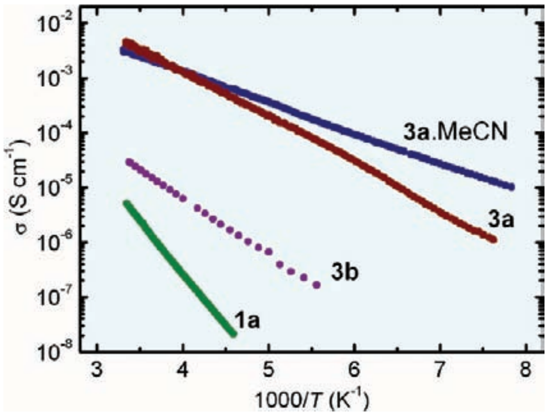

Figure 13. Plots of log σ versus $1/T$ for representative radicals. The derived thermal activation energies are provided in Table 6. Data for **1a** and **3b** were taken from refs 25b and 34, respectively.

while the conductivity of these new radicals remains activated, indicative of a Mott-insulating ground state, the value of E_{act} = 0.11 eV derived for **3a**·MeCN constitutes, to our knowledge, the lowest thermal activation energy ever reported for a neutral $f = {}^1/_2$ radical. In contrast, radicals **1** show E_{act} values in the range 0.40−0.50 eV,[25b] while that of the best of their selenium analogues is lowered to 0.17 eV.[49]

■ DISCUSSION

The semiquinone-bridged bisdithiazolyls **3a** and **3b** constitute the first members of a new class of resonance-stabilized π-radical for use in the design of $f = {}^1/_2$ conductors. Their electrochemical cell potentials E_{cell}, which are lower than those observed for the pyridine-bridged radicals **1a** and **1b**, augur well for improved performance by virtue of a reduced on-site Coulomb repulsion term U. Moreover, in contrast to the pyridine-bridged systems **1**, where the N-alkyl group creates an insulating buffer between neighboring molecules, the carbonyl oxygen atom in **3** plays an active structure-making role, giving rise to tightly packed structures linked by short intermolecular S···O′ contacts. These supramolecular synthons afford a rich variety of novel packing motifs, including the head-over-tail motif found for **3b** and the stacked-ribbon architecture found in **3a**·MeCN (Figure 14). Only in the case of the unsolvated radical **3a** does the packing of the π-stacks resemble the herringbone pattern typically observed for pyridine-bridged radicals **1**.

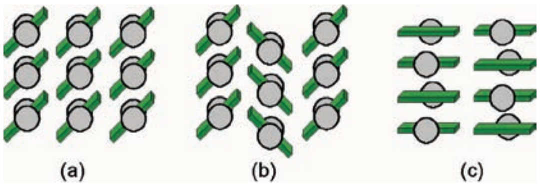

Figure 14. Packing patterns found in **1**, **2**, and **3**: (a) slipped-ribbon π-stacks; (b) herringbone π-stacks; (c) alternating head-over-tail π-stacks.

These new structural motifs give rise to interesting magnetic properties. The head-over-tail π-stacking previously found for **3b** affords remarkably strong FM interactions along the π-stacks, and upon cooling to 4.5 K, the FM chains undergo antiparallel AFM ordering.[34] In the case of **3a** (unsolvated), AFM ordering is also observed, but the unusual crystal structure, with three independent molecules in the asymmetric unit, precludes a detailed interpretation of its magnetic structure, although the orthogonal overlap condition of the π-stacks suggests an FM interaction. Attempts to model the $\chi(T)$ data above 100 K using either a 1D FM or AFM chain $S = {}^1/_2$ model were unsuccessful. This is perhaps not unexpected in view of the fact that there are three distinct π-stacks (**A**, **B**, and **C**), but given this structural complexity, it is surprising that the bulk material is capable of ordering magnetically. The origin of the strong local AFM interactions in the solvated material **3a**·MeCN is a little clearer. The $\chi(T)$ data from 150 to 300 K could be fitted using a molecular-field-modified Bonner−Fisher 1D $S = {}^1/_2$ antiferromagnetically coupled chain model[50] which, when referenced to the Hamiltonian $\hat{H}_{ex} = -2J\hat{\mathbf{S}}_1\cdot\hat{\mathbf{S}}_2$, afforded J and zJ' values of −32.4 and 12.8 cm^{-1} respectively. However, modeling the 2−100 K data produced an equally acceptable fit but with $J = -38.1$ cm^{-1} and $zJ' = 45.2$ cm^{-1}. The variation in and magnitude of the mean-field zJ' term perhaps indicates the inadequacy of the 1D model (the zJ' values are too large) or may simply reflect changes in exchange energies occasioned by contraction of the unit cell upon cooling.

However, the charge transport properties of these semiquinone-bridged materials constitute their most remarkable and appealing features. As a set, structures **3a**, **3a**·MeCN, and **3b** display room-temperature conductivities several orders of magnitude higher than those of their pyridine-based counterparts **1a** and **1b**. The thermal activation energies are also much lower, indeed lower than those observed for selenium-based variants of **1**, where the heavy-atom effect affords improved orbital overlap (a larger W) and a softer core (a lower U). The question therefore arises as to the origin of this improved performance in the semiquinone materials. Is it a result of an intrinsically lower U or an improved bandwidth W, or are there additional features that need to be considered? As noted above, the electrochemical evidence suggests an intrinsically lower *U*, and the π-stacked slipped-ribbon architecture for **3a**·MeCN clearly provides a significant enhancement in *W*. In essence, the operational guidelines provided by the Mott−Hubbard model seem to work, at least qualitatively.

■ SUMMARY AND CONCLUSION

The preparation and characterization of the chloro-substituted semiquinone-bridged bisdithiazolyl radical **3a** takes the neutral radical conductor concept a major step forward. While a metallic state has not been achieved, the two crystalline modifications **3a** and **3a**·MeCN are both Mott insulators, and the acetonitrile adduct nonetheless displays, to our knowledge, the lowest activation energy ever observed for an $f = {}^{1}/_{2}$ single-component system and therefore the smallest Mott−Hubbard gap. It remains to be seen whether the performance of the materials reported here is open to improvement by chemical modification (further variations in R) or the application of physical pressure. In the latter context, we recently described the pressure-induced conversion of selenium-based variants of **1** into weakly metallic states,[30] and the present compounds may respond even more dramatically.

■ EXPERIMENTAL SECTION

General Methods and Procedures. The reagents sulfur monochloride, OMFc, DiMFc, AgOTf, $AgSbF_6$, and 4-chlorophenol (**4a**) were obtained commercially. All were used as received save for OMFc and DiMFc, which were sublimed in vacuo and recrystallized from MeCN before use. The solvents MeCN, EtCN, dichloroethane (DCE), dichloromethane (DCM), carbon disulfide, hexane, and diethyl ether were of at least reagent grade. MeCN and EtCN[51] were dried by distillation from P_2O_5 and CaH_2 and DCM by distillation from P_2O_5. All reactions were performed under an atmosphere of dry nitrogen. Melting points are uncorrected. IR spectra (Nujol mulls, KBr optics) were recorded on a Nicolet Avatar FTIR spectrometer at 2 cm^{-1} resolution, and visible spectra were collected on samples dissolved in MeCN using a PerkinElmer Lambda 35 UV−vis spectrophotometer. ^1H NMR spectra were run on a Bruker Avance 300 MHz NMR spectrometer, and low-resolution electrospray ionization mass spectra were recorded on a Micromass Q-TOF Ultima Global LC/MS/MS system. Elemental analyses were performed by MHW Laboratories (Phoenix, AZ).

Preparation of 4-Chloro-2,6-dinitrophenol (5a). Nitric acid (93.7 g, 1.49 mol) was added dropwise to a solution of **4a** (45.0 g, 0.350 mol) in 300 mL of glacial acetic acid at room temperature. The dark-orange mixture was stirred at 75 °C for 30 min and then poured onto 400 mL of crushed ice. The light-yellow solid was collected by filtration, washed with H_2O, and dried in air to give **5a** with a yield of 66.9 g (0.306 mol, 87%). Recrystallization from 1:1 (v:v) DCM/hexane afforded yellow needles, mp 79−80 °C (lit.[52] 80−81 °C). ^1H NMR ($CDCl_3$): δ 8.29 (s, 2H, Ph), 11.40 (s, 1H, OH).

Preparation of 2,6-Diamino-4-chlorophenol Bishydrochloride (6a). Following the procedure described for 2,6-diaminophenol,[53] tin powder (31.4 g, 0.264 mol) was added in portions to a mixture of **5a** (25.1 g, 0.115 mol) and $SnCl_2 \cdot 2H_2O$ (26.1 g, 0.116 mol) suspended in 100 mL of concentrated HCl at 0 °C and left to stir at 0 °C for 1 h. HCl gas was then passed through the reaction mixture for 2 min, and the resulting precipitate was collected by filtration and washed with 20 mL of concentrated HCl. The product was recrystallized twice from 1:1 (v:v) HCl/H_2O and dried at 110 °C under vacuum to give **6a** as white needles in a yield of 15.7 g (0.0679 mol, 59% yield); dec >230 °C. ^1H NMR (DMSO): δ 6.72 (s, 2H, Ph), 7.61 (s, 7H, NH_3, OH). Anal. Calcd for $C_6H_9Cl_3N_2O$: C, 31.13; H, 3.29; N, 12.10. Found: C, 31.38; H, 3.71; N, 12.26.

Preparation of [3a][Cl]. Sulfur monochloride (11.7 g, 86.6 mmol) was added dropwise to a solution of **6a** (4.01 g, 17.3 mmol) in 100 mL of anhydrous MeCN, and the mixture was heated under gentle reflux overnight. The blue-black solid was filtered off and washed with MeCN, hot DCE, and CS_2 to remove all of the residual sulfur halides. The resulting solid, crude [**3a**][Cl] (R = Cl) was dried in vacuo. Yield 4.22 g (13.4 mmol, 77%); mp >250 °C. IR (cm^{-1}): 1671 (s), 1279 (s), 1097 (m), 1019 (m), 834 (m), 819 (m), 777 (m), 763 (m), 733 (m), 621 (w), 607 (w), 487 (m), 469 (m).

Preparation of [3a][SbF$_6$]. Solid $NOSbF_6$ (3.92 g, 14.8 mmol) was added to a slurry of crude [**3a**][Cl] (4.22 g, 13.4 mmol) in 100 mL of anhydrous MeCN, affording a deep-purple solution that was gently heated at reflux for 1 h and then filtered. The solvent was flash-distilled from the filtrate, leaving [**3a**][SbF_6] as a golden solid (4.62 g, 8.96 mmol, 67.0% yield), which was crystallized from acetic acid or EtCN; mp >250 °C. Anal. Calcd for $C_6N_2S_4OClSbF_6$: C, 13.98; N, 5.43. Found: C, 13.71; N, 5.10. IR (cm^{-1}): 1671 (s), 1281 (s), 1270 (s), 1107 (m), 1025 (m), 857 (w), 841 (m), 874 (m), 654 (s), 559 (w), 490 (w). UV−vis: λ_{max} = 573 nm, $\varepsilon = 1.6 \times 10^4$ L mol^{-1} cm^{-1}. Crystals of the solvate [**3a**][SbF_6]·MeCN suitable for X-ray diffraction work were grown from MeCN.

Preparation of [3a][OTf]. AgOTf (3.42 g, 13.3 mmol) was added to a slurry of crude [**3a**][Cl] (3.82 g, 12.1 mmol) in 100 mL of anhydrous MeCN, affording a deep-purple solution that was gently heated at reflux for 1 h and then filtered to remove a gray precipitate of AgCl. The solvent was flash-distilled from the filtrate, leaving [**3a**][OTf] as a golden solid, which was crystallized from hot MeCN or EtCN as metallic green shards. Yield 3.07 g (7.16 mmol, 59.1%); mp >250 °C. Anal. Calcd for $C_7N_2S_5O_4F_3$: C, 19.60; N, 6.53. Found: C, 19.86; N, 6.61. IR (cm^{-1}): 1683 (s), 4180 (s), 1442 (s), 1412 (m), 1283 (m), 1267 (s), 1264 (s), 1248 (s), 1224 (s), 1175 (s), 1167 (s), 1102 (m), 1028 (s), 857 (w), 839 (m), 785 (m), 758 (w), 640 (m), 635 (m), 576 (w), 517 (m), 486 (w), 472 (w).

Preparation of 3a·MeCN. *Method 1. Bulk Material for Conductivity and Magnetic Measurements.* A solution of [**3a**][OTf] (214 mg, 0.50 mmol) in 30 mL of degassed MeCN (three freeze−pump−thaw cycles) was added to a solution of excess DiMFc (326 mg, 1.00 mmol) in 100 mL of similarly degassed MeCN. After 30 min, the fine microcrystalline precipitate of **3a**·MeCN was filtered off, washed with 5 × 30 mL of MeCN, and dried in vacuo. Yield 140 mg (0.44 mmol, 88%); mp >250 °C. Anal. Calcd for $C_8H_3ClN_3OS_4$: C, 29.95; H, 0.94; N, 13.10. Found: C, 29.98; H, 1.02; N, 13.30. IR (cm^{-1}): 2246 (w, ν(CN)), 1603 (s, br, ν(CO)), 1366 (w), 1311 (m, br), 1117 (m), 997 (m), 952 (m, br), 902 (w), 807 (w), 710 (s), 589 (w), 502 (m), 467 (w), 452 (m).

Method 2. Slow Diffusion for Single Crystals. A solution of [**3a**][SbF_6] (150 mg, 0.291 mmol) in 15 mL of degassed MeCN (four freeze−pump−thaw cycles) was allowed to diffuse slowly into a similarly degassed solution of DiMFc (300 mg, 1.40 mmol) in 15 mL of MeCN. After 15 h, purple needles of **3a**·MeCN (31 mg, 0.11 mmol, 38%) suitable for crystallographic work were collected, washed with MeCN, and dried under a stream of nitrogen.

Preparation of 3a. *Method 1. Bulk Material for Conductivity and Magnetic Measurements.* A solution of [**3a**][OTf] (313 mg, 0.730 mmol) in 30 mL of degassed EtCN (three freeze−pump−thaw cycles) was added to a stirred solution of OMFc (316 mg, 1.09 mmol) in 100 mL of similarly degassed EtCN, yielding a green solution with a crystalline precipitate. After 2 h at room temperature, the purple microcrystalline product was filtered off, washed with EtCN, and dried under vacuum. Yield 174 mg (0.621 mmol, 85% yield); mp >250 °C. Anal. Calcd for $C_6ClN_2OS_4$: C, 25.76; N, 10.01. Found: C, 26.00; N, 9.81. IR (cm^{-1}): 1615 (s), 1115 (m), 994 (s), 905 (m), 831 (m), 811 (m), 734 (s), 604 (w), 584 (w), 499 (m), 465 (m), 445 (m).

Method 2. Slow Diffusion for Single Crystals. A solution of [**3a**][SbF_6] (75 mg, 0.145 mmol) in 15 mL of degassed MeCN (four freeze−pump−thaw cycles) was allowed to diffuse slowly into a similarly degassed solution of OMFc (100 mg, 0.346 mmol) over a 6 h period, affording **3a** (20 mg, 0.071 mmol, 49% yield) as very fine, hairlike needles.

Cyclic Voltammetry. CV was performed using a PINE Bipotentiostat, Model AFCClBP1, with scan rates of 50−250 mV s^{-1} on solutions of [**3a**][OTf] in MeCN (dried by distillation from P_2O_5

and CaH_2) containing 0.1 M tetra-*n*-butyl-ammonium hexafluorophosphate. Potentials were scanned with respect to the quasi-reference electrode in a single-compartment cell fitted with Pt electrodes and referenced to the Fc/Fc^+ couple of ferrocene at 0.38 V vs SCE. The $E_{pa}-E_{pc}$ separation of the reversible couples were within 10% of that of the Fc/Fc^+ couple.[54]

EPR Spectroscopy. The X-band EPR spectrum of **3a** was recorded at ambient temperature on a Bruker EMX-200 spectrometer using a sample of MeCN-solvated or unsolvated radical dissolved in degassed toluene. Hyperfine coupling constants were obtained by spectral simulation using Simfonia[55] and WinSim.

Crystallography. Crystals were glued to glass fibers with epoxy. X-ray data for [**3a**][SbF_6] were collected using ω scans with a Bruker APEX I CCD detector on a D8 three-circle goniometer and Mo Kα (λ = 0.71073 Å) radiation. The data were scanned using Bruker's SMART program and integrated using Bruker's SAINT software.[56] The structure was solved by direct methods using SHELXS-90 and refined by least-squares methods on F^2 using SHELXL-97 incorporated in the SHELXTL suite of programs.[57] X-ray data for the radical **3a**·MeCN were collected using ω scans with a Bruker Microstar Cu rotating-anode (λ = 1.54178 Å) diffractometer equipped with a Proteum 135 CCD detector. The data were integrated with SAINT and scaled with X-SCALE, which is part of the Bruker Proteum software package.[58] Structural solutions[56] and least-squares refinements were conducted using the Olex2 interface[59] to the SHELX suite. The slightly low coverage (93%) reflects the fact that the uncollected high-angle reflections would have required a lot more Cu rotating-anode instrument time, which was not available. The refinement showed no ill effects because of this minor omission. X-ray data for the unsolvated radical **3a** were also collected on a Bruker Proteum-135 CCD system equipped with a Cu MicroSTAR rotating anode (λ = 1.54178 Å). The frames were integrated with the Bruker SAINT software package and corrected for absorption effects using the multiscan method SADABS. The structure was solved and refined using the Bruker SHELXTL software package. In view of the small size of the crystal and the resulting paucity of data, the final R (0.0808) and R_w (0.2027) were not unexpected. Powder X-ray diffraction data on bulk **3a** were collected at ambient temperature on a powder diffractometer equipped with a position-sensitive detector (INEL) using Cu Kα_1 radiation (λ = 1.54056 Å). The total 2θ range was 0–112°, measured in steps of 0.029°. Starting with the space group, unit cell, and molecular coordinates available from the single-crystal data, the unit cell dimensions were refined by Rietveld methods[60] using the GSAS program package.[61]

Magnetic Susceptibility Measurements. DC magnetic susceptibility measurements on **3a**·MeCN and **3a** were performed over the temperature range 2–300 K on a Quantum Design MPMS SQUID magnetometer. Diamagnetic corrections were made using Pascal's constants.[62]

Conductivity Measurements. Temperature-dependent four-probe conductivity measurements on cold pressed pellet samples (1 mm × 1 mm × 5 mm) of **3a**·MeCN and **3a** were performed over the range 140–300 K using an Oxford Instruments MagLab EXA system and home-built equipment. Silver paint (Leitsilber 200) was used to apply the electrical contacts.

Molecular Electronic Structure Calculations. All of the DFT calculations were performed with the Gaussian 09W suite of programs[63] using the (U)B3LYP hybrid functional and polarized split-valence basis sets with triple-ζ [6-311G(d,p)] functions. Full geometry optimization was invoked for the calculation of the total SCF energies of cation, anion, and radical states of **1a** and **3a**, from which the gas-phase IP and EA values were derived. Atomic spin densities ρ and hyperfine coupling constants a_N (in mT) were taken from single-point (U)B3LYP/EPR-III/6-31G(d) calculations at the 6-311G(d,p)-optimized geometries.

Band Structure Calculations. EHT band electronic structure calculations were performed with the Caesar suite of programs[64] using the Coulomb parameters of Baasch, Viste, and Gray[65] and a quasi-split-valence basis set adapted from Clementi and Roetti.[66] The off-diagonal elements of the Hamiltonian matrix were calculated with the standard weighting formula.[67] Atomic positions were taken from crystallographic data. In the case of **3a**·MeCN, the MeCN molecules were not included in the calculations.

■ ASSOCIATED CONTENT

Ⓢ Supporting Information

Complete refs 4a and 63; details of single-crystal X-ray crystallographic data collection and structure refinement and tables of atomic coordinates, bond distances and angles, anisotropic thermal parameters, and hydrogen atom positions (CIF); intermolecular contacts in **3a** and **3a**·MeCN; fitting of magnetic data for **3a**·MeCN; and archival files from G09 calculations. This material is available free of charge via the Internet at http://pubs.acs.org.

■ AUTHOR INFORMATION

Corresponding Author

oakley@uwaterloo.ca

■ ACKNOWLEDGMENTS

We thank the Natural Sciences and Engineering Research Council of Canada (NSERCC) and the Engineering and Physical Sciences Research Council (U.K.) for financial support. We also acknowledge the NSERCC for a Vanier Graduate Scholarship to K.L.

■ REFERENCES

(1) (a) Torrance, J. B. *Acc. Chem. Res.* **1979**, *12*, 79. (b) Garito, A. F.; Heeger, A. J. *Acc. Chem. Res.* **1974**, *7*, 232.

(2) (a) Tanaka, H.; Okano, Y.; Kobayashi, H.; Suzuki, W.; Kobayashi, A. *Science* **2001**, *291*, 285. (b) Kobayashi, A.; Fujiwara, E.; Kobayashi, H. *Chem. Rev.* **2004**, *104*, 5243.

(3) (a) Bendikov, M.; Wudl, F.; Perepichka, D. F. *Chem. Rev.* **2004**, *104*, 4891. (b) Jérome, D. *Chem. Rev.* **2004**, *104*, 5565. (c) Geiser, U.; Schlueter, J. A. *Chem. Rev.* **2004**, *104*, 5203. (d) Yamada, J.; Akutsu, H.; Nishikawa, H.; Kikuchi, K. *Chem. Rev.* **2004**, *104*, 5057. (e) Saito, G.; Yoshida, Y. *Bull. Chem. Soc. Jpn.* **2007**, *80*, 1.

(4) (a) Haddon, R. C.; et al. *Nature* **1991**, *350*, 320. (b) Hebard, A. F.; Rosseinsky, M. J.; Haddon, R. C.; Murphy, D. W.; Glarum, S. H.; Palstra, T. T. M.; Ramirez, A. P.; Kortan, A. R. *Nature* **1991**, *350*, 600. (c) Haddon, R. C. *Acc. Chem. Res.* **1992**, *25*, 127. (d) Allemand, P. M.; Khemani, K. C.; Koch, A.; Wudl, F.; Holczer, K.; Donovan, S.; Gruner, G.; Thompson, J. D. *Science* **1991**, *253*, 301.

(5) (a) Coronado, E.; Galán-Mascarós, J. R.; Gómez-García, C. J.; Laukhin, V. *Nature* **2000**, *408*, 447. (b) Coronado, E.; Day, P. *Chem. Rev.* **2004**, *104*, 5419. (c) Coronado, E.; Giménez-Saiz, C.; Gómez-García, C. J. *Coord. Chem. Rev.* **2005**, *249*, 1776. (d) Coronado, E.; Giménez-Saiz, C.; Gómez-García, C.; Romero, F. M; Tarazón, A. *J. Mater. Chem.* **2008**, *18*, 928.

(6) (a) Sugawara, T.; Komatsu, H.; Suzuki, K. *Chem. Soc. Rev.* **2011**, *40*, 3105. (b) Matsushita, M. M.; Kawakami, H.; Kawada, Y.; Sugawara, T. *Chem. Lett.* **2007**, *36*, 110. (c) Matsushita, M. M.; Kawakami, H.; Sugawara, T.; Ogata, M. *Phys. Rev. B* **2008**, *77*, No. 195208.

(7) (a) Wolf, S. A.; Awschalom, D. D.; Buhrman, R. A.; Daughton, J. M.; von Molnár, S.; Roukes, M. L.; Chtchelkanova, A. Y.; Trege, B. D. M. *Science* **2001**, *294*, 1488. (b) Žutic, I.; Fabian, J.; Das Sarma, S. *Rev. Mod. Phys.* **2004**, *76*, 323. (c) Yoo, J.; Chen, C.; Jang, H. W.; Bark, C. W.; Prigodin, V. N.; Eom, C. B.; Epstein, A. J. *Nat. Mater.* **2010**, *9*, 638. (d) Bader, S. D.; Parkin, S. S. P. *Annu. Rev. Condens. Matter Phys.* **2010**, *1*, 71. (e) Sanvito, S. *Chem Soc. Rev.* **2011**, *40*, 3336.

(8) (a) Rawson, J. M.; Alberola, A.; Whalley, A. *J. Mater. Chem.* **2006**, *16*, 2560. (b) Hicks, R. G. In *Stable Radicals: Fundamentals and Applied Aspects of Odd-Electron Compounds*; Hicks, R. G., Ed.; Wiley: Wiltshire, U.K., 2010; pp 317–380. (c) Ratera, I.; Veciana, J. *Chem. Soc. Rev.* **2012**, *41*, 303.

(9) (a) Haddon, R. C. *Nature* **1975**, *256*, 394. (b) Haddon, R. C. *Aust. J. Chem.* **1975**, *28*, 2333. (c) Haddon, R. C. *Aust. J. Chem.* **1975**, *28*, 2343.

(10) (a) Eley, D. D.; Jones, K. W.; Littler, J. G. F.; Willis, M. R. *Trans. Faraday Soc.* **1966**, *62*, 3192. (b) Inokuchi, H.; Harada, Y.; Maruyama, Y. *Bull. Chem. Soc. Jpn.* **1962**, *35*, 1559.

(11) Hubbard, J. *Proc. R. Soc. London* **1963**, *A276*, 238.

(12) (a) Mott, N. F. *Proc. Phys. Soc. A* **1949**, *62*, 416. (b) Mott, N. F. *Metal−Insulator Transitions*; Taylor and Francis: London, 1990.

(13) In Hartree−Fock theory, this condition becomes $W > (\pi/4)U$. See: Whangbo, M. H. *J. Chem. Phys.* **1979**, *70*, 4763.

(14) (a) Chi, X.; Itkis, M. E.; Patrick, B. O.; Barclay, T. M.; Reed, R. W.; Oakley, R. T.; Cordes, A. W.; Haddon, R. C. *J. Am. Chem. Soc.* **1999**, *121*, 10395. (b) Goto, K.; Kubo, T.; Yamamoto, K.; Nakasuji, K.; Sato, K.; Shiomi, D.; Takui, T.; Kubota, M.; Kobayashi, T.; Yakusi, K.; Ouyang, J. *J. Am. Chem. Soc.* **1999**, *121*, 1619. (c) Mandal, S. K.; Samanta, S.; Itkis, M. E.; Jensen, D. W.; Reed, R. W.; Oakley, R. T.; Tham, F. S.; Donnadieu, B.; Haddon, R. C. *J. Am. Chem. Soc.* **2006**, *128*, 1982. (d) Pal, S. K.; Itkis, M. E.; Tham, F. S.; Reed, R. W.; Oakley, R. T.; Haddon, R. C. *J. Am. Chem. Soc.* **2008**, *130*, 3942. (e) Morita, Y.; Suzuki, S.; Sato, K.; Takui, T. *Nat. Chem.* **2011**, *3*, 197.

(15) (a) Haddon, R. C.; Sarkar, A.; Pal, S. K.; Chi, X.; Itkis, M. E.; Tham, F. S. *J. Am. Chem. Soc.* **2008**, *130*, 13683. (b) Bag, P.; Itkis, M. E.; Pal, S. K.; Donnadieu, B.; Tham, F. S.; Park, H.; Schlueter, J. A.; Siegrist, T.; Haddon, R. C. *J. Am. Chem. Soc.* **2010**, *132*, 2684. (c) Huang, J.; Kertesz, M. *J. Am. Chem. Soc.* **2003**, *125*, 13334. (d) Huang, J.; Kertesz, M. *J. Am. Chem. Soc.* **2007**, *129*, 1634. (e) Bohlin, J.; Hansson, A.; Stafstrom, S. *Phys. Rev. B* **2006**, *74*, No. 155111. (f) Kubo, T.; Katada, Y.; Shimizu, A.; Hirao, Y.; Sato, K.; Takui, T.; Uruichi, M.; Yakushi, K.; Haddon, R. C. *J. Am. Chem. Soc.* **2011**, *133*, 14240.

(16) Saito, G.; Ota, A.; Yoshida, Y.; Maesato, M.; Yamochi, H.; Balodis, K.; Neilands, O.; Khasanov, S.; Tanatar, M. A. *Mol. Cryst. Liq. Cryst.* **2004**, *423*, 99.

(17) Lahti, P. *Adv. Phys. Org. Chem.* **2011**, *45*, 93.

(18) (a) Kinoshita, M.; Turek, P.; Tamura, M.; Nozawa, K.; Shiomi, D.; Nakazawa, Y.; Ishikawa, M.; Takahashi, M.; Awaga, K.; Inabe, T.; Maruyama, Y. *Chem. Lett.* **1991**, *20*, 1225. (b) Tamura, M.; Nakazawa, Y.; Shiomi, D.; Nozawa, K.; Hosokoshi, Y.; Ishikawa, M.; Takahashi, M.; Kinoshita, M. *Chem. Phys. Lett.* **1991**, *186*, 401. (c) Chiarelli, R.; Novak, M. N.; Rassat, A.; Tholence, J. L. *Nature* **1993**, *363*, 147. (d) Alberola, A.; Less, R. J.; Pask, C. M.; Rawson, J. M.; Palacio, F.; Oliete, P.; Paulsen, C.; Yamaguchi, A.; Farley, R. D.; Murphy, D. M. *Angew. Chem., Int. Ed.* **2003**, *42*, 4782.

(19) Peierls, R. C. *Quantum Theory of Solids*; Oxford University Press: London, 1955; p 108.

(20) (a) Cordes, A. W.; Haddon, R. C.; Oakley, R. T. *Adv. Mater.* **1994**, *6*, 798. (b) Oakley, R. T. *Can. J. Chem.* **1993**, *71*, 1775.

(21) (a) Barclay, T. M.; Cordes, A. W.; George, N. A.; Haddon, R. C.; Itkis, M. E.; Mashuta, M. S.; Oakley, R. T.; Patenaude, G. W.; Reed, R. W.; Richardson, J. F.; Zhang, H. *J. Am. Chem. Soc.* **1998**, *120*, 352. (b) Boeré, R. T.; Roemmele, T. L. *Coord. Chem. Rev.* **2000**, *210*, 369. (c) Kaszynski, P. *J. Phys. Chem. A* **2001**, *105*, 7626. (d) Decken, A.; Mailman, A.; Passmore, J.; Rautiainen, J. M.; Scherer, W.; Scheidt, E.-W. *Dalton Trans.* **2011**, *40*, 868.

(22) (a) Bryan, C. D.; Cordes, A. W.; Haddon, R. C.; Glarum, S. H.; Hicks, R. G.; Kennepohl, D. K.; MacKinnon, C. D.; Oakley, R. T.; Palstra, T. T. M.; Perel, A. S.; Schneemeyer, L. F.; Scott, S. R.; Waszczak, J. V. *J. Am. Chem. Soc.* **1994**, *116*, 1205. (b) Bryan, C. D.; Cordes, A. W.; Fleming, R. M.; George, N. A.; Glarum, S. H.; Haddon, R. C.; MacKinnon, C. D.; Oakley, R. T.; Palstra, T. T. M.; Perel, A. S. *J. Am. Chem. Soc.* **1995**, *117*, 6880. (c) Bryan, C. D.; Cordes, A. W.; Goddard, J. D.; Haddon, R. C.; Hicks, R. G.; MacKinnon, C. D.; Mawhinney, R. C.; Oakley, R. T.; Palstra, T. T. M.; Perel, A. S. *J. Am. Chem. Soc.* **1996**, *118*, 330.

(23) ΔH_{disp} is the enthalpy change for the conversion of two gas-phase radicals R into a cation/anion pair, i.e., $2R \leftrightarrows R^+ + R$, and is equal to the difference between the ionization potential (IP) and electron affinity (EA). The cell potential $E_{cell} = E_{1/2}(ox) - E_{1/2}(red)$ is the numerical difference between the half-wave potentials for the oxidation and reduction processes.

(24) Beer, L.; Cordes, A. W.; Haddon, R. C.; Itkis, M. E.; Oakley, R. T.; Reed, R. W.; Robertson, C. M. *Chem. Commun.* **2002**, 1872.

(25) (a) Cordes, A. W.; Haddon, R. C.; Oakley, R. T. *Phosphorus, Sulfur, Silicon Relat. Elem.* **2004**, *179*, 673. (b) Beer, L.; Brusso, J. L.; Cordes, A. W.; Haddon, R. C.; Itkis, M. E.; Kirschbaum, K.; MacGregor, D. S.; Oakley, R. T.; Pinkerton, A. A.; Reed, R. W. *J. Am. Chem. Soc.* **2002**, *124*, 9498.

(26) (a) Brusso, J. L.; Derakhshan, S.; Itkis, M. E.; Kleinke, H.; Haddon, R. C.; Oakley, R. T.; Reed, R. W.; Richardson, J. F.; Robertson, C. M.; Thompson, L. K. *Inorg. Chem.* **2006**, *45*, 10958. (b) Brusso, J. L.; Cvrkalj, K.; Leitch, A. A.; Oakley, R. T.; Reed, R. W.; Robertson, C. M. *J. Am. Chem. Soc.* **2006**, *128*, 15080.

(27) (a) Winter, S. M.; Datta, S.; Hill, S.; Oakley, R. T. *J. Am. Chem. Soc.* **2011**, *133*, 8126. (b) Pivtsov, A. V.; Kulik, L. V.; Makarov, A. Y.; Blockhuys, F. *Phys. Chem. Chem. Phys.* **2011**, *13*, 3873.

(28) Leitch, A. A.; Brusso, J. L.; Cvrkalj, K.; Reed, R. W.; Robertson, C. M.; Dube, P. A.; Oakley, R. T. *Chem. Commun.* **2007**, 3368.

(29) Robertson, C. M.; Leitch, A. A.; Cvrkalj, K.; Reed, R. W.; Myles, D. J. T.; Dube, P. A.; Oakley, R. T. *J. Am. Chem. Soc.* **2008**, *130*, 8414.

(30) Leitch, A. A.; Lekin, K.; Winter, S. M.; Downie, L. E.; Tsuruda, H.; Tse, J. S.; Mito, M.; Desgreniers, S.; Dube, P. A.; Zhang, S.; Liu, Q.; Jin, C.; Ohishi, Y.; Oakley, R. T. *J. Am. Chem. Soc.* **2011**, *133*, 6051.

(31) Leitch, A. A.; McKenzie, C. E.; Oakley, R. T.; Reed, R. W.; Richardson, J. F.; Sawyer, L. D. *Chem. Commun.* **2006**, 1088.

(32) Leitch, A. A.; Reed, R. W.; Robertson, C. M.; Britten, J. F.; Yu, X.; Secco, R. A.; Oakley, R. T. *J. Am. Chem. Soc.* **2007**, *129*, 7903.

(33) Desiraju, G. R. *Angew. Chem., Int. Ed. Engl.* **1995**, *34*, 2311.

(34) Yu, X.; Mailman, A.; Dube, P. A.; Assoud, A.; Oakley, R. T. *Chem. Commun.* **2011**, *47*, 4655.

(35) Initial attempts to prepare [**3a**][Cl] started from 2,6-diaminophenol, but this approach afforded mixtures of [3][Cl] with R = H and Cl. To ensure the formation of a single product, we turned to the use of 4-chloro-2,6-diaminophenol (as its bishydrochloride) as the starting material.

(36) Beer, L.; Britten, J. F.; Clements, O. P.; Haddon, R. C.; Itkis, M. E.; Matkovich, K. M.; Oakley, R. T.; Reed, R. W. *Chem. Mater.* **2004**, *16*, 1564.

(37) Beer, L.; Cordes, A. W.; Haddon, R. C.; Itkis, M. E.; Oakley, R. T.; Reed, R. W.; Robertson, C. M. *Chem. Commun.* **2002**, 1872.

(38) Boeré, R. T.; Moock, K. H. *J. Am. Chem. Soc.* **1995**, *117*, 4755.

(39) Reported as −0.02 V vs SCE by: Hobi, M.; Ruppert, O.; Gramlich, V.; Togni, A. *Organometallics* **1997**, *16*, 1384.

(40) Reported as 0.241 V vs SCE by: Hoh, G. L. J.; McEwen, W. E.; Kleinberg, J. *J. Am. Chem. Soc.* **1961**, *83*, 3949.

(41) (a) Cordes, A. W.; Mingie, J. R.; Oakley, R. T.; Reed, R. W.; Zhang, H. *Can. J. Chem.* **2001**, *79*, 1352. (b) Barclay, T. M.; Beer, L.; Cordes, A. W.; Oakley, R. T.; Preuss, K. E.; Taylor, N. J.; Reed, R. W. *Chem. Commun.* **1999**, 531. (c) Kaszynski, P. *J. Phys. Chem. A* **2001**, *105*, 7615. (d) Makarov, A. Y.; Zhivonitko, V. V.; Makarov, A. G.; Zikirin, S. B.; Bagryanskaya, I. Y.; Bagryansky, V. A.; Gatilov, Y. V.; Irtegova, I. G.; Shakirov, M. M.; Zibarev, A. V. *Inorg. Chem.* **2011**, *50*, 3017. (e) Gritsan, N. P.; Makarov, A. Y.; Zibarev, A. V. *Appl. Magn. Reson.* **2011**, *41*, 449.

(42) Rietveld refinement of powder diffraction data for unsolvated **3a** at 295(2) K using GSAS afforded $a = 48.814(5)$ Å, $b = 3.86053(30)$ Å, $c = 14.1680(15)$ Å, and $V = 2669.92(29)$ Å^3 with $R_p = 0.0434$ and $R_{wp} = 0.0660$.

(43) (a) Bondi, A. *J. Phys. Chem.* **1964**, *68*, 441. (b) Dance, I. *New J. Chem.* **2003**, *27*, 22.

(44) Cozzolino, A. F.; Vargas-Baca, I.; Mansour, S.; Mahmoudkhani, A. H. *J. Am. Chem. Soc.* **2005**, *127*, 3184.

(45) Laves, F.; Baskin, Y. *Z. Kristallogr., Kristallgeom., Kristallphys., Kristallchem.* **1956**, *107*, 337.

(46) In the orthorhombic structures of **3a**·MeCN and **3a**, there is an absolute correspondence between the directions of the real and reciprocal unit cell vectors.

(47) Baker, G. A.; Rushbrooke, G. S.; Gilbert, H. E. *Phys. Rev.* **1964**, *135*, A1272.

(48) The value $\phi = 0.14°$ was determined from the formula $\varphi = \sin^{-1}(M_{\text{spont}}/M_{\text{sat}})$, where M_{sat} was set arbitrarily at 1 $N\beta$, that is, the saturation value ($M_{\text{sat}} = gSN\beta$) for an $S = {}^1/_2$ ferromagnet with a nominal g value of 2.

(49) Leitch, A. A.; Yu, X.; Winter, S. M.; Secco, R. A.; Dube, P. A.; Oakley, R. T. *J. Am. Chem. Soc.* **2009**, *131*, 7112.

(50) Bonner, J. C.; Fisher, M. E. *Phys. Rev. A* **1964**, *135*, 640.

(51) Chai, C. L. L.; Armarego, W. L. F. *Purification of Laboratory Chemicals*, 5th ed.; Butterwirth-Heinemann: New York, 2003.

(52) Zolfigol, M. A.; Madrakian, E.; Ghaemi, E. *Synlett* **2003**, 2222.

(53) Kanamori, D.; Yamada, Y.; Onoda, A.; Okamura, T.; Adachi, S.; Yamamoto, H.; Ueyama, N. *Inorg. Chim. Acta* **2005**, *358*, 331.

(54) Boeré, R. T.; Moock, K. H.; Parvez, M. *Z. Anorg. Allg. Chem.* **1994**, *620*, 1589.

(55) *WinEPR Simfonia*, version 1.25; Bruker Instruments, Inc.: Billerica, MA, 1996.

(56) *SAINT*, version 6.22; Bruker Advanced X-ray Solutions, Inc.: Madison, WI, 2001.

(57) Sheldrick, G. M. *Acta Crystallogr.* **2008**, *A64*, 112.

(58) *Proteum2*, version 2010.1−2; Bruker AXS, Inc.: Karlsruhe, Germany, 2010.

(59) Dolomanov, O. V.; Bourhis, L. J.; Gildea, R. J.; Howard, J. A. K.; Puschmann, H. *J. Appl. Crystallogr.* **2009**, *42*, 339.

(60) Rietveld, H. M. *J. Appl. Crystallogr.* **1969**, *2*, 65.

(61) Larson, A. C.; Von Dreele, R. B. *General Structure Analysis System (GSAS)*; Los Alamos National Laboratory Report LAUR-86-748; Los Alamos National Laboratory: Los Alamos, NM, 1987.

(62) Carlin, R. L. *Magnetochemistry*; Springer: New York, 1986.

(63) Frisch, M. J.; et al. *Gaussian 09*, revision A.02; Gaussian, Inc.: Wallingford, CT, 2009.

(64) *CAESAR: Program for Crystal and Electronic Structure Analysis*, version 2.0.; PrimeColor Software, Inc.: Cary, NC, 1998.

(65) Basch, H.; Viste, A.; Gray, H. B. *Theor. Chim. Acta* **1965**, *3*, 458.

(66) Clementi, E.; Roetti, C. *At. Data Nucl. Data Tables* **1974**, *14*, 177.

(67) Ammeter, J. H.; Bürgi, H. B.; Thibeault, J. C.; Hoffmann, R. *J. Am. Chem. Soc.* **1978**, *100*, 3686.